European Journal of Nuclear Medicine and Molecular Imaging (2019) 46:2380–2391
https://doi.org/10.1007/s00259-019-04430-4

ORIGINAL ARTICLE

Low-calorie sweeteners augment tissue-specific insulin sensitivity in a large animal model of obesity

Charles-Henri Malbert[1] · Michael Horowitz[2] · Richard L. Young[2,3]

Received: 11 February 2019 / Accepted: 9 July 2019 / Published online: 24 July 2019

Abstract

Purposes Whether low-calorie sweeteners (LCS), such as sucralose and acesulfame K, can alter glucose metabolism is uncertain, particularly given the inconsistent observations relating to insulin resistance in recent human trials. We hypothesized that these discrepancies are accounted for by the surrogate tools used to evaluate insulin resistance and that PET ^{18}FDG, given its capacity to quantify insulin sensitivity in individual organs, would be more sensitive in identifying changes in glucose metabolism. Accordingly, we performed a comprehensive evaluation of the effects of LCS on whole-body and organ-specific glucose uptake and insulin sensitivity in a large animal model of morbid obesity.

Methods Twenty mini-pigs with morbid obesity were fed an obesogenic diet enriched with LCS (sucralose 1 mg/kg/day and acesulfame K 0.5 mg/kg/day, LCS diet group), or without LCS (control group), for 3 months. Glucose uptake and insulin sensitivity were determined for the duodenum, liver, skeletal muscle, adipose tissue and brain using dynamic PET ^{18}FDG scanning together with direct measurement of arterial input function. Body composition was also measured using CT imaging and energy metabolism quantified with indirect calorimetry.

Results The LCS diet increased subcutaneous abdominal fat by ≈ 20% without causing weight gain, and reduced insulin clearance by ≈ 40%, while whole-body glucose uptake and insulin sensitivity were unchanged. In contrast, glucose uptake in the duodenum, liver and brain increased by 57, 66 and 29% relative to the control diet group ($P < 0.05$ for all), while insulin sensitivity increased by 53, 55 and 28% ($P < 0.05$ for all), respectively. In the brain, glucose uptake increased significantly only in the frontal cortex, associated with improved metabolic connectivity towards the hippocampus and the amygdala.

Conclusions In miniature pigs, the combination of sucralose and acesulfame K is biologically active. While not affecting whole-body insulin resistance, it increases insulin sensitivity and glucose uptake in specific tissues, mimicking the effects of obesity in the adipose tissue and in the brain.

Keywords Brain connectivity · Compartmental analysis · Glucose uptake · Insulin sensitivity · Miniature pig · Statistical parameter mapping · Sweeteners

This article is part of the Topical Collection on Preclinical Imaging

Electronic supplementary material The online version of this article (https://doi.org/10.1007/s00259-019-04430-4) contains supplementary material, which is available to authorized users.

✉ Charles-Henri Malbert
charles-henri.malbert@inra.fr

[1] Aniscan Unit, Department of Human Nutrition, INRA, 16, le clos, 35590 Saint-Gilles, France

[2] Center of Research Excellence in Translating Nutrition to Good Health, The University of Adelaide, Adelaide 5005, Australia

[3] Nutrition & Metabolism, South Australia Health & Medical Research Institute, Adelaide 5000, Australia

Abbreviations

LCS	Low-calorie sweeteners
^{18}FDG	^{18}Fluorodeoxyglucose
PET-CT	Positron emission tomography coupled with computed tomography
MRglu	Metabolic rate for glucose utilization
ROI	Region of interest
VOI	Volume of interest

Introduction

The outcomes of studies relating to both the acute and chronic effects of low-calorie sweeteners (LCS) on glucose homeostasis support the concept that they are not physiologically inert [1, 2]. However, whether LCS affect metabolism remains controversial [3]. For example, in 2018, three controlled trials [4–6] investigated the impact of several weeks of consumption of three popular LCS on insulin sensitivity. Two studies, 2 and 4 weeks in duration, which investigated the addition of sucralose at or below the acceptable daily intake found significant reductions in total insulin sensitivity with [5] and without [4] a reduction in insulin secretion. In contrast, Bonnet et al. [6], who investigated a mixture of aspartame and acesulfame K corresponding to the amount provided by two servings of commercial soft drinks, failed to identify changes in insulin sensitivity despite a 12-week intervention time and the inclusion of subjects with a larger body mass index (BMI). Surprisingly, no studies have investigated insulin sensitivity after the prolonged use of sucralose-acesulfame K, particularly as this mixture has been promoted by the food industry following increasing public concern related to potential adverse effects of aspartame [7].

The mechanisms underlying metabolic effects of sucralose and acesulfame K are poorly characterized, but the outcomes of several rodent experiments [8, 9] together with in vitro testing [10–12] indicate that acesulfame K and sucralose may modify glucose metabolism through several pathways. For example, in the rat, acesulfame K doubled plasma insulin concentrations after a single IV dose and increased insulin release in isolated rat pancreatic islets [10, 13]. A comparable increase in insulin release was also observed after the addition of sucralose in an identical experimental set-up [14]. However, when given orally for about a year in mice, acesulfame K had no effect on insulin sensitivity or body weight [9]. Increases in glucose intestinal uptake have been demonstrated for acesulfame K and sucralose alike in Caco 2 cells [12], probably via increased expression of SGLT-1 and glucose transporter 2 [15–17]. Aside from these effects on glucose metabolism, there is evidence to suggest several other targets for sucralose and acesulfame K. For example, in mice, prolonged oral supplementation with acesulfame K impaired cognitive function together with inhibition of glycolysis and neurosynaptic abnormalities in hippocampal neurons [9, 18]. In human and rat cells, acesulfame has been reported to stimulate adipogenesis and suppress lipolysis [11].

Several tissues, including the liver, skeletal muscle and adipose tissue, exhibit a reduction in insulin-dependent glucose uptake in obesity [19]. Although insulin resistance develops concurrently in multiple organs, its progression differs between them [20]. Differential effects of LCS on tissue-specific insulin resistance may, therefore, account for the counterintuitive impact of LCS on metabolic homeostasis [21]. Indeed, there is evidence of impaired glucose tolerance [22] in the absence of weight changes after prolonged LCS intake [23], although neither changes in glucose uptake nor insulin sensitivity have been assessed using quantitative imaging approaches [24].

We, therefore, determined the effect of prolonged (12 weeks) supplementation with a sucralose-acesulfame K mixture on whole-body and organ-specific, insulin-dependent glucose uptake and insulin sensitivity in a large animal model of obesity. We performed our experiments in obese animals [25] given that obese subjects represent prevalent users of LCS [26] and chose the Yucatan mini-pig because it is known to develop obesity in response to a high-fat/sucrose diet [25]. We hypothesized that prolonged consumption of two commonly partnered LCS in diet beverages would affect insulin resistance and glucose uptake. We quantified the effects of LCS supplementation on whole-body, brain, liver, duodenum, skeletal muscle and subcutaneous and visceral fat insulin sensitivities using PET CT imaging. This was achieved during insulin stimulation designed to mimic that observed during a nutrient meal [27] via an euglycemic hyperinsulinemic clamp. The latter, unlike simple insulin stimulation, allowed stable glycemia for extended periods, a prerequisite for quantitative glucose uptake measurement using PET [28]. Specific attention was given to the impact of LCS on brain function since (i) insulin appears to increase brain glucose uptake only in the setting of obesity [27] and (ii) habitual LCS consumption has been shown to modify brain networks relevant to the regulation of glycemia [18]. Non-oxidative glucose metabolism was also quantified using indirect calorimetry, and body composition with CT imaging to further characterize the metabolic status of the animals [25].

Materials and methods

Animals

Twenty adult Yucatan mini-pigs, aged 3 years, were fed a high-fat/high-sucrose pellet diet (4024 kcal/kg feed) supplied at 150% of the recommended caloric intake for 5 months to induce morbid obesity before the onset of the experiment (Table 1). Food was provided once a day and water supplied ad libitum. Energy intake was maintained during the entire experiment. The animals were housed individually in 2-m^2 cages, enriched with toys to encourage physical exercise. Visual and limited physical contact between animals was permitted by the design of the cages. The experiment was conducted according to ethical standards of European and French legislation, and with the approval of the Rennes Animal Ethics Committee (R-2011-MO-01).

Experimental protocol

Mini-pigs were divided into two groups ($n = 10$ each) matched for weight, age and sex. The amount of obesogenic diet ingested spontaneously by each animal during 1 week was recorded prior to experimentation. During the 3-month experimental period, this amount of food was supplied to control for potential differences in palatability between the control and

Table 1 Phenotypic and metabolic characteristics of mini-pigs at 12 weeks after LCS supplementation

	Control diet group	LCS diet group
Sex ratio	1	1
Body weight before intervention (kg)	86.4 ± 1.38	87.9 ± 1.85
Body weight after intervention (kg)	92.8 ± 1.19	93.2 ± 0.98
Total abdominal fat mass before intervention (kg)	24.0 ± 2.21	24.4 ± 2.98
Total abdominal fat mass after intervention (kg)	26.4 ± 3.21	31.3 ± 1.15*
Visceral fat mass before intervention (kg)	11.5 ± 0.91	11.2 ± 0.89
Visceral fat mass after intervention (kg)	12.2 ± 2.91	11.1 ± 2.14
Fasting energy expenditure (kcal/day)	1054 ± 29.1	993 ± 80.1
Energy expenditure during clamp (kcal/day)	1321 ± 70.9	1235 ± 95.0
Glucose oxidation rate (mg/kg/min)	1.9 ± 0.24	1.4 ± 0.63

*Indicates a significant difference between groups at $P \leq 0.05$. $N = 10$ per group

LCS diets. The control diet group was maintained on the same high-fat, high-carbohydrate pellet diet throughout, while the LCS diet group received the same diet enriched with a mixture of two LCS: sucralose (92 mg daily) and acesulfame K (52 mg daily) for 3 months, corresponding to daily consumption of ~500 mL of diet beverage in humans [29]. Both groups ate the total amount of food given daily.

One week before the end of the experiment, the mini-pigs were scanned by CT (HiSpeed NX/i; GE Medical Systems, Milwaukee, WI, USA) to quantify subcutaneous and abdominal fat [30]. Briefly, subcutaneous and intra-abdominal fat volumes were obtained after averaging CT slices performed at T13 and L2 levels. Segmentation of subcutaneous and intra-abdominal fat was performed semi-automatically using ITK-SNAP software. Total abdominal fat was estimated as the sum of subcutaneous and intra-abdominal fat. During the same anesthesia, an endoscope was passed into the duodenum to deliver 70 mL of a radio-opaque medium (Micropaque Scanner, 5 g of barium sulfate per mL, Guerbet). Once the compound filled the duodenum from the ligament of Treitz to the duodenal bulb, a high-resolution 3D scan was performed to identify the location of the duodenum relative to three fiducial markers sutured to the skin at precisely 90° from each other. This was done to allow accurate localization of the duodenum while not affecting the attenuation image for the PET procedure.

Euglycemic-hyperinsulinemic clamp procedure

PET imaging was performed after a 12-h fast during a euglycemic-hyperinsulinemic clamp. Insulin (Actrapid, Novo Nordisk, Denmark) and 20% glucose were infused using a catheter placed extemporaneously in a saphenous vein. Insulin was diluted in 50 mL saline plus 0.5% homologous blood and infused at 120 $mU.kg^{-1}.h^{-1}$ [25] without a priming dose. Arterial blood samples were obtained every 5 min and measured by the glucose oxidase method on a rapid analyzer (Analox GM9 Analyzer; Analox Instruments, London, UK). The clamp was computer-controlled with custom software [31]. For each clamp, the plateau was considered to have been achieved when differences in glucose uptake rate and glycemia were less than 5% in three consecutive samples. In most animals, this was reached within 2 h after the onset of the clamp. Access to the arterial supply was achieved with a Seldinger-type catheter (RS+A50K10SQ, Terumo, France) inserted extemporaneously under echo guidance (M Turbo, Sonosite, France) in either the left or right femoral artery. Arterial and plasma glucose concentrations were determined in duplicate on a multiparametric analyzer (Konelab 20i, Thermo Fisher Scientific). Plasma insulin concentrations were measured in clamp studies using an ST-AIA-Pack IRI reagent kit, with a quantification limit of 0.5 $\mu U.mL^{-1}$ and intra-assay coefficient of variation less than 2% from 12 to 200 $\mu U.mL^{-1}$. Insulin clearance was calculated by dividing the rate of insulin infusion by the mean steady-state plasma insulin concentration. Whole-body glucose uptake and insulin sensitivity were calculated using AniMate software [25]. Endogenous glucose production was estimated using the procedure described by Iozzo et al. in pigs [32] and was used to confirm the absence of hepatic glucose production during the clamp.

Energy expenditure measurement

Energy expenditure and carbohydrate oxidation rate were measured after 12-h fasting by indirect calorimetry before and during the plateau of the euglycemic hyperinsulinemic clamp. A breath-to-breath metabolic analyzer (Quark RMR, Cosmed) was attached to a non-rebreathing ventilator (Siemens SAL 900) to measure the difference between inspired and expired VO_2 and VCO_2 [33]. The calorimeter was calibrated daily using gas of certified O_2 partial pressure (spO_2) and CO_2 partial pressure ($spCO_2$) composition, and the flowmeter was also calibrated using a 3-L syringe. Determinations of energy expenditure and carbohydrate oxidation rate were obtained, as described from calorimetric measurements for at least 15 min, until the reading was stable at

±10% [34]. Non-oxidative glucose utilization was calculated by subtracting the rate of glucose oxidation during a given time period from the total rate of glucose uptake obtained with the clamp during the same period.

PET imaging

PET images were acquired during the euglycemic-hyperinsulinemic clamp with an ECAT EXACT HR scanner (CTI/Siemens). Mini-pigs were anesthetized with isoflurane (measured minimum alveolar concentration 1.8 vol) in an air/O_2 mixture. The ventilation parameters were set to maintain $spCO_2$ at 4.3 ± 2% and spO_2 at 98%, or more, while the insufflation pressure was less than 20 mmHg (ADU-AS/3, GE, France). Homeothermy was maintained using a forced-hot-air blanket (Bair Hugger, 3M, France). A transmission scan of 5 min was performed with three rotating pin sources containing ^{68}Ge before the emission scan to correct for tissue attenuation. At the glucose perfusion plateau of the clamp, ^{18}fluorodeoxyglucose (FDG, ~370 MBq, IBA France) was injected intravenously over 30 s using an automated injector; the amount of ^{18}FDG injected was subsequently calculated through measurements of the residuals from the injecting syringe, extension lines and sampling vial. The PET scanning started from the brain (4 × 30 s, 3 × 60 s, 10 × 300 s frames) followed by the liver (5 × 300 s frames), abdomen (5 × 300 s frames) and legs (5 × 300 s frames). Concurrently with the PET scanning, arterial blood radioactivity was recorded continuously for the first 13 min after ^{18}FDG injection using an in-line device coupled with a gamma ray detector [31]. Blood was drawn at a rate of 4 mL/min through a computer-controlled peristaltic pump. Subsequently, arterial blood and plasma samples were withdrawn once during each time frame and measured using an automatic gamma counter (Wizard 1470, Perkin Elmer). The in-line blood sampling device and automatic gamma counter were both cross-calibrated on a daily basis before the experiment against the PET scanner using an ^{18}F water-filled phantom of 5 L as a reference. In addition, data originating from the in-line blood sampler were corrected for dispersion error caused by the length of the arterial sampling line according to Munk et al. [35]. Composite arterial input function was built from these measurements using AniMate software [31].

All image data were corrected for dead time, decay and photon attenuation. PET images were reconstructed by filtered back-projection and smoothed with a Hanning 0.5-Hz filter. This provided a spatial resolution of 8.5 mm full-width at half maximum transaxially and axially. Reconstructed images of the brain were displayed in a 128 × 128 × 63 voxel format, each voxel measuring 0.64 × 0.64 × 2.42 mm. These values were equal to 128 × 128 × 63 voxels, where each voxel measured 2.57 × 2.57 × 2.42 mm for the liver, fat and muscle. Glucose uptake rates obtained initially in units of volume were converted to units of weight using the following densities: 1 g/mL for brain tissue, 1.05 g/mL for liver, 1.06 g/mL for skeletal muscle and 0.95 g/mL for adipose tissue.

Image analysis

Glucose uptake rates were obtained for each organ through model or Patlak analyses of regions of interest (VOI) data and arterial input function using PMod software (Switzerland). VOIs for the liver, the duodenum, the muscle and the subcutaneous/visceral fat were obtained initially from the semiautomatic or entirely manual segmentation of the organs based on CT performed after the PET imaging and after the co-registration of the CT on the PET-averaged images based on the fiducial markers (Fig. 1). This was done using ITK-

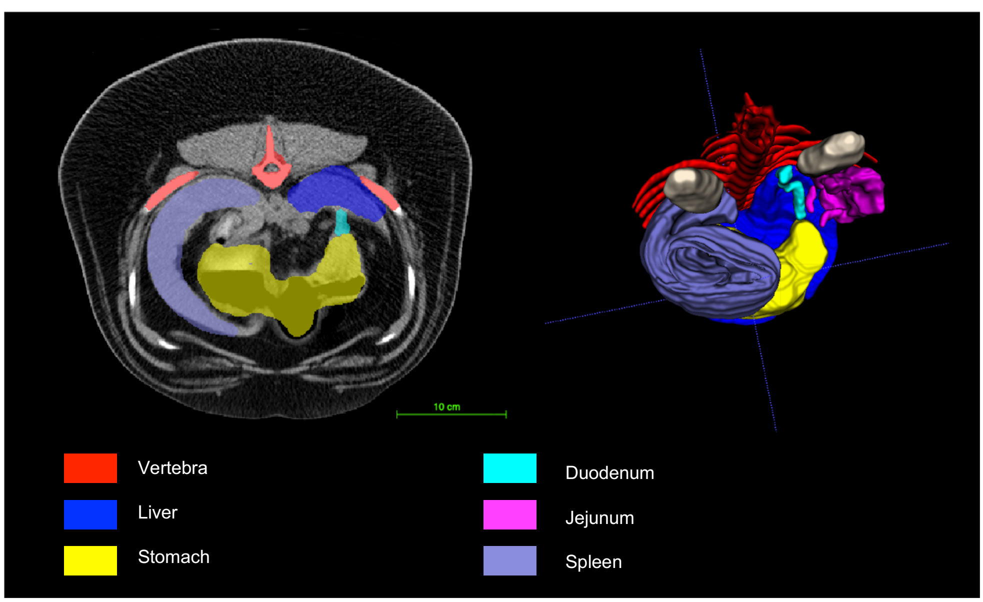

Fig. 1 Segmentation of the porcine abdominal organ using ITK-snap. Segmentation was performed semi-manually from CT images, and the resulting mesh was then converted into PMOD-compatible VOIs for Patlak graphical analyses of glucose uptake. Note the clear delineation of the duodenum in contrast to the indistinct proximal jejunum, explaining why glucose uptake was not calculated for the jejunum

Snap software to generate a 3D mesh of these organs [36]. These meshes were converted subsequently into PMod-compatible VOIs. When uncertainty about the accuracy of the segmentation was considered unacceptable (e.g. visual difference between the CT and PET boundaries of the organ), the size of the VOIs was reduced manually to increase the probability of accurate segmentation. The manual refinement step of the mesh was extended to the liver hilum to exclude the large vessels at their entrance in the tissue from the liver VOI. This was done individually in each animal. VOIs at the brain level were obtained automatically by co-registration of the PET brain image with a dynamic PET template co-registered with our 3D brain atlas [37]. The following lumped constants (LC) were used to take into account the differences in affinity between FDG and native glucose: 0.45 for brain [38], 1 for liver [39], 1.15 for duodenum [40], 1.14 for adipose tissue [41] and 1.2 for skeletal muscle [42]. A classical 3 K model was used for the brain, while a Patlak graphical analysis was performed for the liver, duodenum, abdominal subcutaneous fat and visceral fat. The difference in the analysis workflow reflected the absence of early (0–60 min) images for these organs, unlike the brain, for which these scans were obtained. Transfer constants K1, k2 and k3 were used to characterize the model at the brain level, where K1 represents mainly transport and k3 phosphorylation. Muscle glucose uptake was averaged over the two thighs. Similarly, subcutaneous fat MRglu obtained from the abdominal scan was averaged from the left and right sides. Due to the limited size of the visceral fat pad on the left side, MRglu for visceral fat was calculated unilaterally. Insulin sensitivity was calculated for each organ from the value of glucose uptake divided by the mean arterial glycemia during the scan of the organ under investigation multiplied by the difference of insulin concentrations from basal to clamp conditions [20].

Changes in brain glucose uptake that did not extend to large brain areas were evaluated with pixel-wise modeled brain volumes reconstructed from the raw PET images, and arterial input function using PXMod software with the Patlak method [43]. Similarly, brain maps coded for transfer coefficients were built using a two-tissue compartment model with the basis function method of Hong and Fryer [44]. These maps were analyzed for differences at a voxel level using SPM [Statistical Parametric Mapping] (SPM12, Wellcome Trust Centre for Neuroimaging, London, UK). Metabolic connectivity analysis [45] was performed using NetPET software on quantitative CMRglu images to identify significant network components (NetPET V1, L. Moro, M. Veronese and M. Arcolin). Brain networks were visualized with BrainNet Viewer [46] and the circular graph Matlab subroutine using regions extracted from the pig brain atlas according to the structural volume's definitions of Hammers et al. in humans [47].

Statistical analysis

Data are presented as mean ± standard error of the mean (SEM) and were compared using an unpaired t test with Prism 7 (GraphPad Software, USA) unless otherwise indicated. Differences were considered statistically significant if $P \leq 0.05$. Correlation matrices were used to evaluate possible relationships between organ-specific glucose uptake. Pearson r correlation coefficients were computed and presented using a heat map. Statistical analysis of brain uptake rate was compared using paired t tests with SPM12 at a significance level of $P \leq 0.001$, and were FDR (false detection rate)-corrected to exclude random brain activation. Brain connectivity matrices were thresholded using the corresponding probability matrices for $P \leq 0.001$.

Results

Insulin sensitivity and body composition

After the dietary intervention, the body weight of the LCS diet group was similar to that of the control diet group ($P > 0.05$, Table 1). There was a change in body composition, due to a 20% increase in total abdominal fat mass in the LCS compared to control group ($P = 0.03$). This reflected an increase in subcutaneous fat, since the amount of visceral (including perirenal) fat was unchanged (P > 0.05, Table 1). Energy expenditure was not modified by LCS, either in the fasting condition or during the clamp.

Fasting glucose and insulin were comparable between the two groups. In both groups, mean plasma glucose concentration was 6.4 ± 0.4 mmol/L during the euglycemic hyperinsulinemic clamp

Table 2 Biochemical characteristics of mini-pigs after 12 weeks of LCS supplementation

		Control diet group	LCS diet group
Fasting	Plasma glucose (mmol/L)	6.0 ± 0.17	6.6 ± 0.49
	Plasma insulin (μU/mL)	5.2 ± 1.71	5.5 ± 1.45
Clamp	Whole-body insulin sensitivity (dL/kg.min/μU/mL*1E^{-3})	3.2 ± 0.29	3.1 ± 0.48
	Whole-body glucose uptake (μmol.min^{-1}.kg^{-1})	19.5 ± 1.36	20.2 ± 1.48
	Metabolic clearance rate of insulin (mL.min^{-1}.kg^{-1})	3.33 ± 0.091	2.38 ± 0.103*
	Endogenous glucose production (μmol.min^{-1}.kg^{-1})	2.41 ± 0.646	−12.9 ± 1.118*

* Indicates a significant difference between groups at $P \leq 0.05$. N = 10 per group

(Table 2), while plasma insulin concentrations during the clamp were not different in the LCS versus control group (774 ± 91 vs. 633 ± 36 μU/mL, $P = 0.135$). Consequently, whole-body insulin sensitivity and whole-body glucose uptake were unchanged, but insulin clearance was reduced by ≈ 40% in the LCS versus control group ($P = 0.011$, Table 2). In both groups, endogenous glucose production was suppressed during the clamp, with a negligible fraction present in the control group only (Table 2).

Organ-specific glucose uptake

LCS supplementation did not affect whole-body glucose uptake; however, glucose uptake increased significantly in the brain (29%), liver (66%), duodenum (57%) and visceral fat (40%) in the LCS compared to the control group (Table 3). These increases in glucose uptake translated to an increased insulin sensitivity for the brain (28%), liver (55%) and duodenum (53%).

The higher glucose uptake was accounted for by parallel increases in glucose transport (K1) in the brain. In contrast to the brain, glucose uptake was unchanged in skeletal muscle and abdominal subcutaneous fat (Table 3).

Correlation analysis of organ-specific glucose uptake showed a reciprocal, and diet-dependent, relationship between glucose uptake in brain and liver ($r = -0.812$ versus 0.908 for control and LCS groups, respectively; $P = 0.009$). A similar relationship between glucose uptake in the duodenum and liver was also evident, albeit as a trend ($P = 0.081$, Fig. 2).

Regional metabolic changes in the brain

Glucose uptake in the brain was higher in the LCS diet group compared to the control diet group (20.8 ± 1.0 vs. 16.1 ± 1.0, $P = 0.0346$). This reflected changes in the dorsolateral prefrontal cortex, the sole brain structure with differential activation between the two groups ($P \leq 0.0001$, FDR-corrected, Fig. 3). The ROI-based analysis confirmed the SPM analysis and established that the local change in glucose uptake was the immediate outcome of an increased inward flux (K1) within the dorsolateral prefrontal cortex (0.113 ± 0.014 vs. 0.082 ± 0.007 mL.min^{-1}, Fig. 4). Small volume correction performed on striatal areas failed to identify significant changes in brain activity between groups, despite increased statistical power.

Metabolic connectivity analysis demonstrated a marked increase in connectivity between the hippocampal amygdaloid complex and the frontal structures for the LCS group only. There was also a significant relationship between the hippocampal amygdaloid complex and the anterior cingulate area (Fig. 5).

Discussion

This is the first study to quantify the effect of chronic administration of a low-dose sucralose-acesulfame K mixture on insulin sensitivity and glucose uptake in organs critical for glucose homeostasis. We observed an increase in insulin sensitivity in the brain, liver, duodenum and visceral fat resulting from an increase in glucose uptake in these organs. That these changes did not affect whole-body insulin sensitivity is not surprising given that skeletal muscle uptake, the major contributor of whole-body glucose uptake and insulin sensitivity [19], was unaffected by LCS supplementation. Furthermore, the metabolic activity of the dorsolateral prefrontal cortex was increased together with metabolic connectivity between frontal areas and the hippocampal amygdaloid complex in the LCS-treated mini-pigs. The LCS supplement we used can be regarded as physiological, given that it represents the content

Table 3 Glucose uptake and insulin sensitivity in brain, liver, duodenum, skeletal muscle and both subcutaneous and visceral fat after 12 weeks of LCS supplementation

		Control diet group	LCS diet group
Glucose uptake (μmol.min^{-1}.100 g^{-1})	Brain	16.1 ± 0.97	20.8 ± 0.96*
	Liver	9.8 ± 0.44	16.1 ± 0.69*
	Duodenum	7.6 ± 0.32	12.0 ± 1.25*
	Muscle	3.2 ± 0.45	3.2 ± 0.12
	Subcutaneous fat	0.6 ± 0.20	0.5 ± 0.04
	Visceral fat	0.6 ± 0.11	0.9 ± 0.19*
Insulin sensitivity (dL/kg.min/μU/mL*1E^{-3})	Brain	6.3 ± 0.30	8.1 ± 0.36*
	Liver	3.8 ± 0.45	5.7 ± 0.41*
	Duodenum	2.8 ± 0.17	4.5 ± 0.18*
	Muscle	1.2 ± 0.10	1.1 ± 0.16
	Subcutaneous fat	0.2 ± 0.20	0.1 ± 0.07
	Visceral fat	0.2 ± 0.19	0.3 ± 0.12

* Indicates a significant difference between groups at $P \leq 0.05$

Glucose uptake was calculated from compartment modeling for the brain, while it was obtained from Patlak graphical analyses for the remaining organs

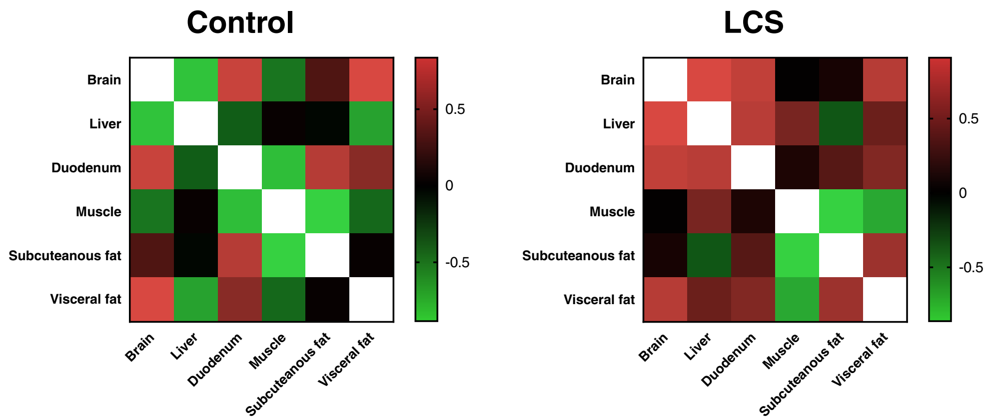

Fig. 2 Heat map matrix of Pearson coefficients for the correlation of glucose uptake in brain, liver, duodenum, muscle and abdominal fat tissues. LCS supplementation reversed the correlation matrices for brain–liver interactions compared to the control group, with similar changes noted in duodenum–liver interactions. Correlation matrices were used to evaluate the possible relationships between organ-specific glucose uptake. Pearson *r* correlation coefficients were computed and presented using a heat map

of 500 mL of carbonated soft drink, and approximately 20% of the daily intake for sucralose and 4% of the daily intake for acesulfame K considered acceptable by the US Food and Drug Administration (FDA) and the Joint FAO/WHO [Food and Agriculture Organization/World Health Organization] Expert Committee on Food Additives. The stimulation of incretin release from L-cells by sucralose is known to be nonlinear [48], which may explain, at least in part, why earlier studies employing sucralose doses many times greater than the usual daily intake failed to identify metabolic effects.

Arguably, the most important outcome of our study was that in obese mini-pigs, sucralose-acesulfame K supplementation increases insulin sensitivity of the brain, liver and duodenum, without affecting the whole-body insulin sensitivity. These observations are consistent with studies in healthy [6] and obese [49] subjects reporting no effect of long-term LCS supplementation on whole-body insulin sensitivity. Nevertheless, our results differ from those of Lertrit et al. [4]. In line with the improved tissue-specific insulin sensitivity, we showed a reciprocal and LCS-dependent relationship between glucose uptake in brain and liver. In the control group, glucose uptake was negatively related in these two organs, but positively related in LCS-treated mini-pigs (such that an increase in liver glucose uptake was linked to higher brain uptake). There was, however, a striking divergence between whole-body and organ-specific glucose uptake. Glucose uptake in skeletal muscle, the major organ determining whole-body glucose uptake [20], was not affected, and it is, accordingly, not surprising that the augmented glucose uptake in the brain, liver, duodenum and visceral fat failed to have a significant effect on whole-body glucose uptake, given the small volume of these organs. Assessment of glucose

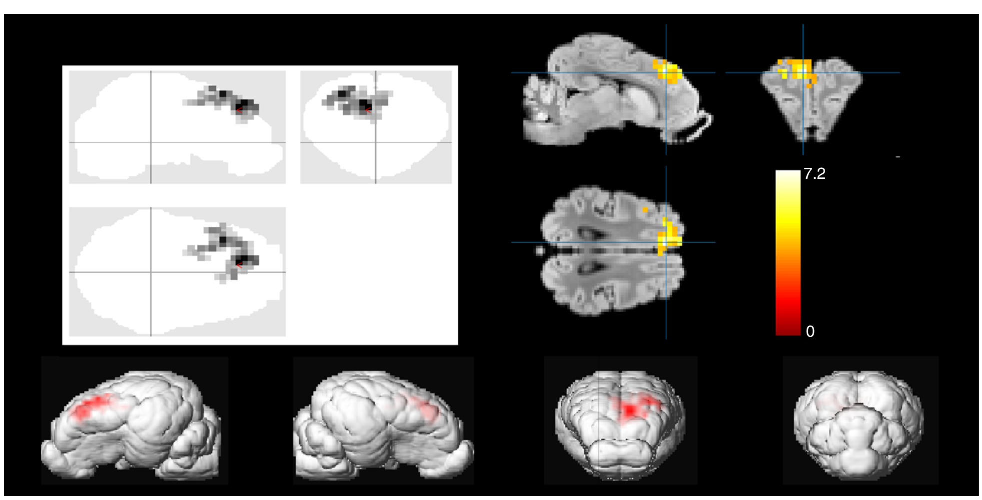

Fig. 3 Statistical comparison within the brain glucose metabolism map obtained during insulin stimulation in control and LCS groups. Statistical analysis was performed on voxel-based glucose uptake-coded images. T values were thresholded at FDR $P \leq 0.0001$, cluster level-corrected. Graphical representation was obtained using XJview. Grey-scale image background was co-registered to T maps and represents the MRI used in our brain atlas for the pig (Saikali et al. 2010). Brain glass image (top left panel) was obtained for the pig brain using a beta version of the small animal molecular imaging toolbox (SAMIT; D. Vallez Garcia) [61]. Note activation within the dorsolateral prefrontal cortex only

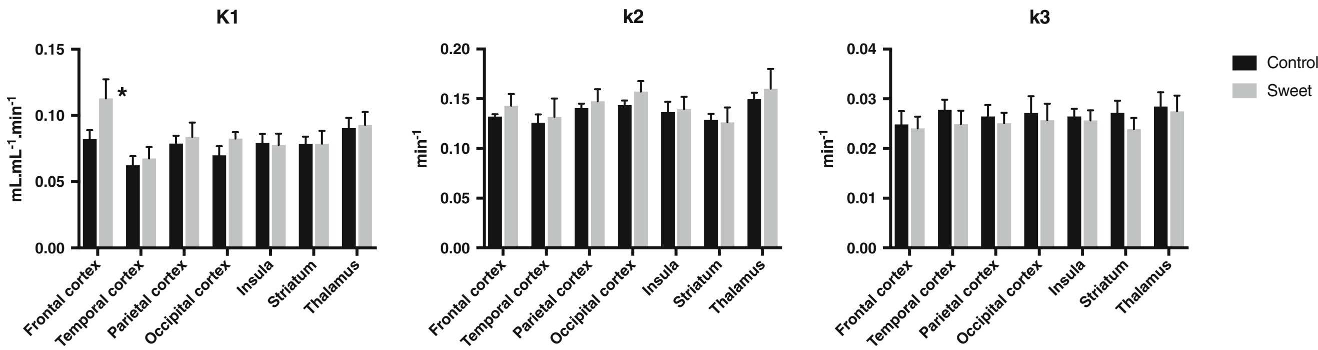

Fig. 4 Brain regional changes in transfer coefficients induced by insulin stimulation in control and LCS groups. K1 represents the transport across the blood-brain barrier and trans-membrane transport. k2 quantifies the retrograde transfer from the cell to blood, while k3 defines the amount of phosphorylation. Note that K1 was altered only in the frontal cortex. *Indicates a difference between control and LCS group ($P < 0.05$). $N = 10$ animals in each group; error bars represent SEM

uptake in the gut is complicated by the fact that the mucosa is more glucose-avid than the external layers [50], with the duodenum being the most amenable to contrast-enhanced CT due to its relatively fixed location. For these reasons, we could not extrapolate duodenal glucose uptake to more distal parts of the gut, or calculate whole-gut glucose uptake.

We demonstrated that chronic exposure to LCS enhanced metabolic activity in the dorsolateral prefrontal cortex. This observation appears robust given that (i) the effect size was large, (ii) ROI-based analysis confirmed the specific pattern and (iii) a priori analysis on the striatum failed to show differences. Dorsal prefrontal functioning is linked to the capacity to exert self-control over food intake upon exposure to appetitive food cues [51], and increased activity occurs in response to viewing of palatable foods [52]. In the current study, this increased activity was sustained and may be linked to the increased metabolic connectivity in the LCS group (which involved frontal structures and extended to the hippocampus and amygdala). Our observations contrast with our original hypothesis, i.e. that an LCS-enriched diet would reduce brain

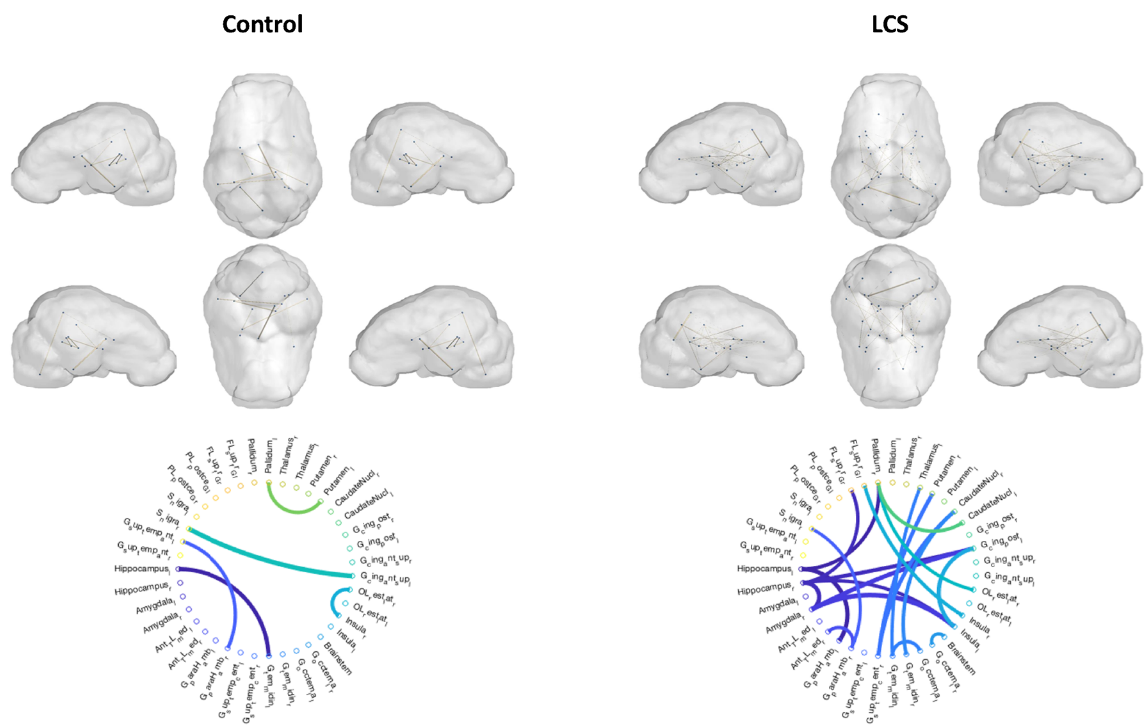

Fig. 5 Metabolic connectivity analysis for control and LCS groups. Metabolic connectivity matrices were calculated using NetPET software. Top panel - Components were presented using BrainNet Viewer with a threshold of $P \leq 0.001$ on the probability map associated with the correlation map. The unconnected nodes were not represented. The thickness of the edges symbolizes the intensity of the correlation. Bottom panel - The same correlation matrices are represented as circular graphs for which the colors denote the intensity of the correlation. Note the substantial increase in brain connectivity for the LCS group with special reference to the amygdala, the hippocampus and the frontal lobe. Abbreviations for nodes are given in supplementary Table S1

connectivity akin to cognitive impairments observed in degenerative diseases [53] and, to a lesser extent, in morbidly obese patients [54]. Rather, ROI, SPM and connectivity-based analyses gave congruous information and provided strong support of a more metabolic active forebrain in LCS-treated obese animals. These results can be compared with those published by our group in obese vs. lean miniature pigs of identical breed using the same PET quantitative measurements of brain metabolism during a comparable euglycemic hyperinsulinemic clamp condition [27]. While obesity was less marked in these younger pigs, brain glucose uptake was also increased by 36% in obese vs. lean animals, a difference of the same order to that observed in the LCS diet group versus control diet group (22%). Since an increase in brain glucose uptake was also observed in obese [55] and insulin-resistant [56] humans compared to lean volunteers, the increase in brain glucose uptake induced by an LCS diet is likely to be detrimental. Furthermore, in both studies, the origin of the increased glucose uptake was identical e.g. an increase in K1 transfer coefficient indicative of larger glucose inward flux involving the transfer from the blood-brain barrier and the extracellular to the intra-cellular space. However, our voxel-based SPM analyses showed that the brain structures responsible for the overall change in increased glucose uptake were not strictly identical: core recollection network for Bahri et al. [27] and dorsolateral prefrontal cortex in the LCS diet group. However, the connectivity analysis identified the same network, yet with different intensity between connecting nodes. In both experimental conditions, the prefrontal cortex, the amygdala and the hippocampus were engaged.

Total abdominal fat increased by 20% in the LCS group reflecting an increase in subcutaneous fat only. Such an increase, without a parallel increase in visceral fat, is uncommon in animal models of diet-induced obesity, but changes in fat deposition in obese patients receiving LCS for 6 months have been reported [49]. As a crude approximation, the product of tissue mass and glucose uptake can be used to calculate tissue-based glucose uptake. Using these figures, there was a gain of 6 μmol of glucose uptake in fat in the LCS versus control group, while uptake for lean/muscle tissue was reduced by 21 μmol of glucose. We recognize that lean tissue mass may have exceeded that of muscle, resulting in an overestimation of lean tissue total glucose uptake. Nevertheless, it is likely that the increased glucose uptake in abdominal fat was counterbalanced, at least partially, by the decrease observed in muscle, so that there was no difference in whole-body glucose uptake between the groups. The same calculation can be used to investigate the imbalanced glucose uptake observed for subcutaneous and visceral fat induced by the LCS diet. Glucose uptake was unchanged in subcutaneous fat, but subcutaneous fat weight increased. The opposite situation was evident for visceral fat with unchanged weight, but increased glucose uptake. Nevertheless, whole-body glucose uptake due to adipose tissue only increased by 30% (visceral) and 42% (subcutaneous), respectively. A similar, yet less marked alteration, in total glucose uptake has been observed in obese vs. lean patients [57].

It is probable that differences in glucose uptake and insulin sensitivity between diets were amplified by obesity, and that different results might have been observed in lean animals. For example, brain glucose uptake was unaffected by insulin in lean miniature pigs, while it is potentiated in obese pigs [27]. The same feature has been also demonstrated in humans for the brain [58]. However, we decided to perform our experiment in obese animals given that obese subjects represent prevalent users of LCS [26]. To what extend the detrimental effects of LCS on glucose uptake and insulin sensitivity were related to BMI remains uncertain.

Our study has methodological limitations which are inherent in the chronic LCS supplementation paradigm. First, we measured glucose uptake during insulin stimulation, given its physiological relevance, rather than in the fasting state [25]. However, "gold-standard" clamp measurement of insulin sensitivity required the use of such an experimental paradigm that has been applied successfully both in animals [27] and humans [58]. Second, for technical reasons, we investigated the duodenum only, and did not measure glucose uptake in other gut regions. Indeed, the duodenum, an organ with proximal and distal ligaments, is sufficiently anatomically stable to perform dynamic PET imaging, unlike the jejunum. Similarly, we used a liver VOI that included most of the organ instead of using several spherical VOI as classically performed in humans [60]. Indeed, while the position of the liver VOI has little impact on calculation of glucose uptake so far they were both located within the right lobe [59], this is probably not the case in the pig. We observed a significant anisotropy in glucose uptake that is more efficiently handled by a large VOI enclosing a substantial portion of the organ. Furthermore, due to major anatomical differences between the porcine and human liver, it was not feasible to apply human guidelines [60] for drawing liver VOI, as the left lobe is larger than the right. Third, potential changes in gut microbiota due to LCS were not assessed, and may be relevant given that dysbiosis due to LCS has been associated with impaired glucose tolerance in mice [2]. Finally, anesthesia has the potential to reduce organ metabolism, especially in the brain. However, the minimal alveolar concentration of isoflurane was monitored and tuned in real time throughout the experiment to minimize the possibility of a difference between groups.

Conclusions

We demonstrated increased insulin sensitivity and augmented glucose uptake in the brain, liver and duodenum, organs pivotal to glucose homeostasis, in LCS supplemented mini-pigs.

Whole-body glucose uptake in adipose tissue was also increased in response to the LCS diet, a feature also evident in obese subjects. These effects were not associated with a parallel change in whole-body insulin sensitivity most likely because muscle glucose uptake, a major contributor to whole-body insulin sensitivity, was comparable in LCS and control groups. Chronic consumption of LCS was also shown to increase the metabolism of the dorsolateral prefrontal cortex via a modification of glucose transport, and increased connectivity between the hippocampus, the amygdala and frontal areas. This increased connectivity together with the increased brain glucose uptake observed in the LCS diet group are consistent with the alterations in brain metabolism identified in diet-induced obese pigs [27] and obese subjects [55]. Accordingly, these changes are indicative of detrimental consequences of chronic consumption of LCS, despite unchanged whole-body insulin sensitivity.

Acknowledgements The authors thank staff of the UEPR unit for animal care, Mickael Genissel, Julien Georges, Alain Chauvin, Francis Le Gouevec, and Vincent Piedvache. We also thank Paula Aneb and Emilie Lebrun for their involvement in running the Aniscan imaging, and Raphael Comte (Pegase unit) for insulin measurements. The authors also thank Eric Bobillier for the development of the in-line radiation detector and robotic feeders.

Author Contributions C-H.M. planned the experiments, conducted the studies, analyzed the data and wrote the manuscript. R.Y. and M.H. were involved in planning the experiments, writing the manuscript and interpretation of the data. C-H.M. is the guarantor of this work and, as such, had full access to all the data in the study and takes responsibility for the integrity of the data and the accuracy of the data analysis.

Funding The study was conducted within the Aniscan Imaging Center (Aniscan, INRA), which is supported by BPIFrance within the Investments for the Future Program.

Compliance with ethical standards

Disclosure of potential conflicts of interest C-H. Malbert declares that he has no conflict of interest. M. Horowitz declares that he has no conflict of interest. R. Young declares that he has no conflict of interest.

Ethical approval All applicable international, national and/or institutional guidelines for the care and use of animals were followed.

References

1. Pepino MY, Tiemann CD, Patterson BW, Wice BM, Klein S. Sucralose affects glycemic and hormonal responses to an oral glucose load. Diabetes Care. 2013;36:2530–5.
2. Suez J, Korem T, Zeevi D, Zilberman-Schapira G, Thaiss CA, Maza O, et al. Artificial sweeteners induce glucose intolerance by altering the gut microbiota. Nature. 2014;514:181–6.
3. Suez J, Korem T, Zilberman-Schapira G, Segal E, Elinav E. Non-caloric artificial sweeteners and the microbiome: findings and challenges. Gut Microbes. 2015;6:149–55.
4. Lertrit A, Srimachai S, Saetung S, Chanprasertyothin S, Chailurkit L-O, Areevut C, et al. Effects of sucralose on insulin and glucagon-like peptide-1 secretion in healthy subjects: A randomized, double-blind, placebo-controlled trial. Nutrition. 2018;55-56:140–5.
5. Romo-Romo A, Aguilar-Salinas CA, Brito-Córdova GX, Gómez-Díaz RA, Almeda-Valdes P. Sucralose decreases insulin sensitivity in healthy subjects: a randomized controlled trial. Am J Clin Nutr. 2018;108:485–91.
6. Bonnet F, Tavenard A, Esvan M, Laviolle B, Viltard M, Lepicard EM, et al. Consumption of a Carbonated Beverage with High-Intensity Sweeteners Has No Effect on Insulin Sensitivity and Secretion in Nondiabetic Adults. J Nutr. 2018;148:1293–9.
7. Hess EL, Myers EA, Swithers SE, Hedrick VE. Associations Between Nonnutritive Sweetener Intake and Metabolic Syndrome in Adults. J Am Coll Nutr. 2018:1–7.
8. Liang Y, Steinbach G, Maier V, Pfeiffer EF. The effect of artificial sweetener on insulin secretion. 1. The effect of acesulfame K on insulin secretion in the rat (studies in vivo). Horm Metab Res. 1987;19:233–8.
9. Cong WN, Wang R, Cai H, Daimon CM, Scheibye-Knudsen M, Bohr VA, et al. Long-term artificial sweetener acesulfame potassium treatment alters neurometabolic functions in C57BL/6J mice. PLoS One. 2013;8:e70257.
10. Malaisse WJ, Vanonderbergen A, Louchami K, Jijakli H, Malaisse-Lagae F. Effects of artificial sweeteners on insulin release and cationic fluxes in rat pancreatic islets. Cell Signal. 1998;10:727–33.
11. Simon BR, Parlee SD, Learman BS, Mori H, Scheller EL, Cawthorn WP, et al. Artificial sweeteners stimulate adipogenesis and suppress lipolysis independently of sweet taste receptors. J Biol Chem. 2013;288:32475–89.
12. Zheng Y, Sarr MG. Effect of the artificial sweetener, acesulfame potassium, a sweet taste receptor agonist, on glucose uptake in small intestinal cell lines. J Gastrointest Surg. 2013;17:153–8 discussion p. 158.
13. Liang Y, Maier V, Steinbach G, Lalić L, Pfeiffer EF. The effect of artificial sweetener on insulin secretion. II. Stimulation of insulin release from isolated rat islets by Acesulfame K (in vitro experiments). Horm Metab Res. 1987;19:285–9.
14. Nakagawa Y, Nagasawa M, Yamada S, Hara A, Mogami H, Nikolaev VO, et al. Sweet taste receptor expressed in pancreatic β-cells activates the calcium and cyclic AMP signaling systems and stimulates insulin secretion. PLoS One. 2009;4:e5106.
15. Mace OJ, Affleck J, Patel N, Kellett GL. Sweet taste receptors in rat small intestine stimulate glucose absorption through apical GLUT2. J Physiol. 2007;582:379–92.
16. Moran AW, Al-Rammahi MA, Arora DK, Batchelor DJ, Coulter EA, Daly K, et al. Expression of Na+/glucose co-transporter 1 (SGLT1) is enhanced by supplementation of the diet of weaning piglets with artificial sweeteners. Br J Nutr. 2010;104:637–46.
17. Smith K, Karimian-Azari E, LaMoia TE, Hussain T, Vargova V, Karolyi K, et al. T1R2 receptor-mediated glucose sensing in the upper intestine potentiates glucose absorption through activation of local regulatory pathways. Mol Metab. 2018.
18. Burke MV, Small DM. Physiological mechanisms by which non-nutritive sweeteners may impact body weight and metabolism. Physiol Behav. 2015;152:381–8.
19. Honka M-J, Latva-Rasku A, Bucci M, Virtanen KA, Hannukainen JC, Kalliokoski KK, et al. Insulin-stimulated glucose uptake in skeletal muscle, adipose tissue and liver: a positron emission tomography study. Eur J Endocrinol. 2018;178:523–31.
20. Goodpaster BH, Bertoldo A, Ng JM, Azuma K, Pencek RR, Kelley C, et al. Interactions among glucose delivery, transport, and phosphorylation that underlie skeletal muscle insulin resistance in obesity and type 2 Diabetes: studies with dynamic PET imaging. Diabetes. 2014;63:1058–68.

21. Swithers SE. Artificial sweeteners produce the counterintuitive effect of inducing metabolic derangements. Trends Endocrinol Metab. 2013;24:431–41.
22. Swithers SE, Laboy AF, Clark K, Cooper S, Davidson TL. Experience with the high-intensity sweetener saccharin impairs glucose homeostasis and GLP-1 release in rats. Behav Brain Res. 2012;233:1–14.
23. Collison KS, Makhoul NJ, Zaidi MZ, Saleh SM, Andres B, Inglis A, et al. Gender dimorphism in aspartame-induced impairment of spatial cognition and insulin sensitivity. PLoS One. 2012;7:e31570.
24. Lammertsma AA. Forward to the Past: The Case for Quantitative PET Imaging. J Nucl Med. 2017;58:1019–24.
25. Malbert C-H, Picq C, Divoux J-L, Henry C, Horowitz M. Obesity-associated alterations in glucose metabolism are reversed by chronic bilateral stimulation of the abdominal vagus nerve. Diabetes. 2017;66:848–57.
26. Sylvetsky AC, Welsh JA, Brown RJ, Vos MB. Low-calorie sweetener consumption is increasing in the United States. Am J Clin Nutr. 2012;96:640–6.
27. Bahri S, Horowitz M, Malbert CH. Inward Glucose Transfer Accounts for Insulin-Dependent Increase in Brain Glucose Metabolism Associated with Diet-Induced Obesity. Obesity (Silver Spring). 2018.
28. Boellaard R. Standards for PET Image Acquisition and Quantitative Data Analysis. J Nucl Med. 2009;50:11S–20S.
29. Ilback N-G, Alzin M, Jahrl S, Enghardt-Barbieri H, Busk L. Estimated intake of the artificial sweeteners acesulfame-K, aspartame, cyclamate and saccharin in a group of Swedish diabetics. Food Addit Contam. 2003;20:115–26.
30. Val-Laillet D, Blat S, Louveau I, Malbert CH. A computed tomography scan application to evaluate adiposity in a minipig model of human obesity. Br J Nutr. 2010;104:1719–28.
31. Malbert C-H. AniMate-An open source software for absolute PET quantification. Annual Congress of the European Association of Nuclear Medicine. 2016:43.
32. Iozzo P, Gastaldelli A, Järvisalo MJ, Kiss J, Borra R, Buzzigoli E, et al. 18F-FDG assessment of glucose disposal and production rates during fasting and insulin stimulation: a validation study. J Nucl Med. 2006;47:1016–22.
33. Rehal MS, Fiskaare E, Tjäder I, Norberg Å, Rooyackers O, Wernerman J. Measuring energy expenditure in the intensive care unit: a comparison of indirect calorimetry by E-sCOVX and Quark RMR with Deltatrac II in mechanically ventilated critically ill patients. Crit Care. 2016;20:54.
34. Golay A, DeFronzo RA, Ferrannini E, Simonson DC, Thorin D, Acheson K, et al. Oxidative and non-oxidative glucose metabolism in non-obese type 2 (non-insulin-dependent) diabetic patients. Diabetologia. 1988;31:585–91.
35. Munk OL, Keiding S, Bass L. A method to estimate dispersion in sampling catheters and to calculate dispersion-free blood time-activity curves. Med Phys. 2008;35:3471–81.
36. Yushkevich PA, Piven J, Hazlett HC, Smith RG, Ho S, Gee JC, et al. User-guided 3D active contour segmentation of anatomical structures: significantly improved efficiency and reliability. Neuroimage. 2006;31:1116–28.
37. Saikali S, Meurice P, Sauleau P, Eliat PA, Bellaud P, Randuineau G, et al. A three-dimensional digital segmented and deformable brain atlas of the domestic pig. J Neurosci Methods. 2010;192:102–9.
38. Poulsen PH, Smith DF, Ostergaard L, Danielsen EH, Gee A, Hansen SB, et al. In vivo estimation of cerebral blood flow, oxygen consumption and glucose metabolism in the pig by [15O]water injection, [15O]oxygen inhalation and dual injections of [18F]fluorodeoxyglucose. J Neurosci Methods. 1997;77:199–209.
39. Iozzo P, Jarvisalo MJ, Kiss J, Borra R, Naum GA, Viljanen A, et al. Quantification of liver glucose metabolism by positron emission tomography: validation study in pigs. Gastroenterology. 2007;132:531–42.
40. Honka H, Mäkinen J, Hannukainen JC, Tarkia M, Oikonen V, Teräs M, et al. Validation of [18F]fluorodeoxyglucose and positron emission tomography (PET) for the measurement of intestinal metabolism in pigs, and evidence of intestinal insulin resistance in patients with morbid obesity. Diabetologia. 2013;56:893–900.
41. Virtanen KA, Peltoniemi P, Marjamäki P, Asola M, Strindberg L, Parkkola R, et al. Human adipose tissue glucose uptake determined using [(18)F]-fluoro-deoxy-glucose ([(18)F]FDG) and PET in combination with microdialysis. Diabetologia. 2001;44:2171–9.
42. Peltoniemi P, Lönnroth P, Laine H, Oikonen V, Tolvanen T, Grönroos T, et al. Lumped constant for [(18)F]fluorodeoxyglucose in skeletal muscles of obese and nonobese humans. Am J Physiol Endocrinol Metab. 2000;279:E1122–30.
43. Patlak CS, Blasberg RG, Fenstermacher JD. Graphical evaluation of blood-to-brain transfer constants from multiple-time uptake data. *J Cereb Blood Flow Metab*. 1983;3:1–7.
44. Hong YT, Fryer TD. Kinetic modelling using basis functions derived from two-tissue compartmental models with a plasma input function: general principle and application to [18F]fluorodeoxyglucose positron emission tomography. Neuroimage. 2010;51:164–72.
45. Yakushev I, Drzezga A, Habeck C. Metabolic connectivity. Curr Opin Neurol. 2017;30:677–85.
46. Xia M, Wang J, He Y. BrainNet Viewer: a network visualization tool for human brain connectomics. PLoS One. 2013;8:e68910.
47. Hammers A, Allom R, Koepp MJ, Free SL, Myers R, Lemieux L, et al. Three-dimensional maximum probability atlas of the human brain, with particular reference to the temporal lobe. Hum Brain Mapp. 2003;19:224–47.
48. Pepino MY. Metabolic effects of non-nutritive sweeteners. Physiol Behav. 2015;152:450–5.
49. Maersk M, Belza A, Stødkilde-Jørgensen H, Ringgaard S, Chabanova E, Thomsen H, et al. Sucrose-sweetened beverages increase fat storage in the liver, muscle, and visceral fat depot: a 6-mo randomized intervention study. Am J Clin Nutr. 2012;95:283–9.
50. Mäkinen J, Hannukainen JC, Karmi A, Immonen HM, Soinio M, Nelimarkka L, et al. Obesity-associated intestinal insulin resistance is ameliorated after bariatric surgery. Diabetologia. 2015;58:1055–62.
51. Hare TA, Camerer CF, Rangel A. Self-control in decision-making involves modulation of the vmPFC valuation system. Science. 2009;324:646–8.
52. Weygandt M, Mai K, Dommes E, Ritter K, Leupelt V, Spranger J, et al. Impulse control in the dorsolateral prefrontal cortex counteracts post-diet weight regain in obesity. Neuroimage. 2015;109:318–27.
53. Lee SH, Zabolotny JM, Huang H, Lee H, Kim YB. Insulin in the nervous system and the mind: Functions in metabolism, memory, and mood. Mol Metab. 2016;5:589–601.
54. Cheke LG, Bonnici HM, Clayton NS, Simons JS. Obesity and insulin resistance are associated with reduced activity in core memory regions of the brain. Neuropsychologia. 2017;96:137–49.
55. Tuulari JJ, Karlsson HK, Hirvonen J, Hannukainen JC, Bucci M, Helmiö M, et al. Weight loss after bariatric surgery reverses insulin-induced increases in brain glucose metabolism of the morbidly obese. Diabetes. 2013;62:2747–51.
56. Hirvonen J, Virtanen KA, Nummenmaa L, Hannukainen JC, Honka MJ, Bucci M, et al. Effects of insulin on brain glucose metabolism in impaired glucose tolerance. Diabetes. 2011;60:443–7.
57. Virtanen KA, Lönnroth P, Parkkola R, Peltoniemi P, Asola M, Viljanen T, et al. Glucose uptake and perfusion in subcutaneous

and visceral adipose tissue during insulin stimulation in nonobese and obese humans. J Clin Endocrinol Metab. 2002;87:3902–10.
58. Iozzo P. Metabolic imaging in obesity: underlying mechanisms and consequences in the whole body. Ann N Y Acad Sci. 2015;1353: 21–40.
59. Viner M, Mercier G, Hao F, Malladi A, Subramaniam RM. Liver SULmean at FDG PET/CT: interreader agreement and impact of placement of volume of interest. Radiology. 2013;267:596–601.
60. Boellaard R, Delgado-Bolton R, Oyen WJ, Giammarile F, Tatsch K, Eschner W, et al. European Association of Nuclear Medicine EANM: FDG PET/CT: EANM procedure guidelines for tumour imaging: version 2.0. Eur J Nucl Med Mol Imaging. 2015;42: 328–54.
61. Vállez Garcia D, Casteels C, Schwarz AJ, Dierckx RA, Koole M, Doorduin J. A standardized method for the construction of tracer specific PET and SPECT rat brain templates: validation and implementation of a toolbox. PLoS One. 2015;10:e0122363.